NeuroImage 50 (2010) 396–408

Contents lists available at ScienceDirect

NeuroImage

journal homepage: www.elsevier.com/locate/ynimg

Anatomical and functional parcellation of the human lateral premotor cortex

Ricarda I. Schubotz [a,b,*], Alfred Anwander [a], Thomas R. Knösche [a], D. Yves von Cramon [a,b], Marc Tittgemeyer [b]

[a] Max Planck Institute for Human Cognitive and Brain Sciences, Leipzig, Germany
[b] Max Planck Institute for Neurological Research, Cologne, Germany

ARTICLE INFO

Article history:
Received 5 August 2009
Revised 10 November 2009
Accepted 15 December 2009
Available online 24 December 2009

Keywords:
Cortex parcellation
Connectivity
Diffusion-weighted imaging (DWI)
Functional magnetic resonance imaging (fMRI)
Precentral gyrus
Premotor cortex

ABSTRACT

The lateral premotor cortex (PM) of the macaque monkey is an anatomically multifaceted area, which serves multiple sensorimotor and cognitive functions. While evidence for the functional organization of human premotor cortex accumulates, much less is known about the underlying anatomical properties of this brain region. We used diffusion tractography and functional magnetic resonance imaging (fMRI) to investigate whether the precentral gyrus in humans can be segregated on the basis of anatomical connectivity and of functional activation in a set of cognitive and motor tasks. Tractographic data suggested a distinction between ventral and dorsal premotor cortex, and furthermore inferior and superior subparcellation of both. Functional MRI data corroborated these four areas, showing that anatomical parcellation predicts the distribution of functional activation and vice versa (preliminary evidence). These results may encourage the application of combining diffusion tractography and fMRI *in vivo* in order to shed light on the correspondence of brain function and anatomy.

Introduction

Evidence has accumulated that the human lateral premotor cortex (PM), subserves not only sensorimotor transformation and motor control, but also attentional and cognitive functions (for an overview, see Schubotz and von Cramon, 2003). A systematic task-dependent localization of the activations found within this area implies a functionally multifaceted brain region. However, the functional analysis of the human PM, and the human cortex in general, is still limited by the fact that insights in the correspondence between function and microstructure, which is taken to correspond to functional units, have been inaccessible so far. That is because, until the emergence of diffusion-weighted imaging (DWI), individual microstructural maps could be derived only postmortem. Macrostructure, i.e., sulci and gyri, are accessible *in vivo*, but do not provide reliable information about functional borders, because changes in cortical microstructure (and hence function) do not necessarily respect cortical macrostructure. Moreover, both micro- and macrostructure are subject to considerable inter- and intraindividual variability (Ono et al., 1990; Rademacher et al., 1993; Roland and Zilles 1996). Hence, a crucial yet unresolved question concerns how many functionally and structurally distinct fields there are in the human lateral premotor cortex.

Cortex parcellation based on diffusion-weighted imaging and tractography capitalizes on the view that differences in anatomical connectivity of brain areas signal for a functional segregation (Behrens & Johansen-Berg, 2005; Johansen-Berg & Behrens, 2006; Johansen-Berg et al., 2004; Anwander et al., 2007). Here, we use diffusion tractography and functional magnetic resonance imaging (fMRI) to investigate *in vivo* whether distinct patterns of connectivity can be found to segregate subregions of the human lateral premotor cortex, and if so, whether these fields are reflected by functional specificity.

Anatomical and functional research in PM of the macaque monkey (area 6, Brodmann 1909) implies PM of the convexity to be subdivided into two major fields, a ventral PM and a dorsal PM (Barbas and Pandya 1987, Dum and Strick, 1991, Ghosh and Gattera, 1995, Rizzolatti et al., 1998, Tanne-Gariepy et al., 2002). Correspondingly, a ventral and a dorsal PM are suggested in humans as well, the border between which is however still a matter of debate (Rizzolatti et al., 2002, Preuss et al., 1996). In fact, Tomassini and colleagues (2007) reported the distinction of a ventral and a dorsal PM based on diffusion tractography, but mostly, evidence for an anatomical parcellation of the human PCG stems from functional studies (for reviews, see Schubotz & von Cramon 2003, Schubotz 2004). However, since a further structural and functional subdivision running orthogonally in rostrocaudal direction has been suggested and often reconfirmed in macaques, resulting in a rostroventral (F5), a caudoventral (F4), a rostrodorsal (F7) and a caudodorsal (F2) field (cf. Geyer et al., 2000), we tested whether our data would support four distinct fields on the lateral convexity as well. Human imaging studies suggest the distinction of at least three functionally distinct fields in lateral PM (Picard & Strick, 2001; Schubotz & von Cramon, 2003). While these confirm a role of dorsal PM in spatial tasks and for

* Corresponding author. Max Planck Institute for Neurological Research, Motor Cognition Group, Gleueler Strasse 50, 50931 Köln, Germany. Fax: +49 (0)221 4726 298.
E-mail address: schubotz@nf.mpg.de (R.I. Schubotz).

1053-8119/$ – see front matter © 2009 Elsevier Inc. All rights reserved.
doi:10.1016/j.neuroimage.2009.12.069

ventral PM in object-related tasks, as in macaques, the inferiormost portion of ventral PM seems to be particularly relevant for processing rhythm and pitch (Schubotz & von Cramon, 2001, 2002; Schubotz et al., 2003, Wolfensteller et al., 2007). Hence, previous functional studies point to a complex parcellation of the human PCG, but it remains an open question as to whether or not structural and corresponding functional compartments can be identified. The present study aimed to further this issue by using diffusion tensor imaging (DTI) and fMRI. Notably, these methods were conducted independently, i.e., DTI data were not used to direct fMRI analysis or vice versa, but in an overlapping sample of subjects in order to determine whether or not there is congruence in the outcomes on structure and function. We first examined whether PM subregions can be identified using diffusion tractography; then we proceeded to assess functional (motor and cognitive) specialization of different sectors of PM (cf. Johansen-Berg et al., 2004 for a comparable approach to the supplementary motor area). To this end, we conducted three experiments (see Methods for details) in the same subjects from which we also collected diffusion weighted imaging data. Experiments employed paradigms that are well established in human and macaque research on premotor function.

In Experiment 1, we aimed to localize two subregions of the primary motor cortex within each hemisphere together with their respective premotor contributions. Subjects were instructed to move their tongue or their fingers according to visual stimuli presented on the screen. Regarding premotor activations, we expected widespread and overlapping activations for tongue and hand movement; however, based on previous findings (summarized in Schubotz & von Cramon, 2003), we expected a direct task contrast to reveal tongue movements to dominate hand movements in the ventral PCG, whereas the opposite should hold true for the dorsal PCG.

In Experiment 2, subjects were asked to attend to the order of serially presented stimuli, either with respect to rhythmical, object-based, or spatial properties. This so-called serial prediction task (SPT, Schubotz, 1999) has been found to reliably engage distinct subregions of the lateral premotor cortex in the absence of motor requirements (Schubotz & von Cramon, 2001; Schubotz et al., 2003; Schubotz, 2004). Following previous findings, we hypothesized rhythmic predictions to engage the inferior ventral PCG, object-based prediction the superior ventral PCG, and spatial predictions the dorsal PCG. Note that (1) these differences, as for Experiment 1, were expected to be revealed by direct task contrasts, i.e., to reflect a weighting or dominance of task-activation relationships rather than absolute differences; and that (2) labels “inferior ventral,” “superior ventral” and “dorsal” are assigned as coarse classifications within each precentral area as revealed by imaging findings cited above (Schubotz, 2004).

In Experiment 3, subjects watched short video clips showing either a pointing or a grasping action towards artifacts. Since movement/action observation has been found to draw on different premotor portions depending on which body part is engaged (Sakreida et al., 2005, Buccino et al., 2001), and according to findings in the macaque reporting differential premotor activity in reaching and grasping (Caminiti et al., 1999, Rizzolatti, 1987), observation of pointing was expected to draw more on dorsal PCG than observation of grasping/manipulation, whereas the opposite pattern was expected for the ventral PCG.

Materials and methods

Diffusion-weighted imaging

Subjects

Ten right-handed subjects (21–33 years, mean 26.1 years, 5 females) took part in the diffusion data acquisition. Participants gave written consent before being included in testing. All participants were right-handed, had normal or corrected-to-normal vision, and were native German speakers. No participant had a history of neurologic, psychiatric, or other major medical disorder. No participant was taking medication at the time of measurement. The experimental standards were approved by the local ethics committee of the University of Leipzig (Leipzig, Germany). Data were handled anonymously.

Data acquisition and preprocessing

Diffusion-weighted data and high-resolution 3-dimensional (3D) T1- and T2-weighted images were acquired on a Siemens 3T Trio scanner with an 8-channel array head coil and maximum gradient strength of 40 mT/m. The diffusion-weighted data were acquired using spin-echo echo planar imaging (EPI) (TR = 12 s, TE = 100 ms, 72 axial slices, resolution $1.72 \times 1.72 \times 1.7$ mm, no cardiac gating). A GRAPPA technique (red.-factor 2.0) was chosen as parallel imaging scheme. Diffusion weighting was isotropically distributed along 60 directions (b-value = 1000 s/mm^2). Additionally, seven data sets with no diffusion weighting were acquired initially and interleaved after each block of 10 diffusion weighted images as anatomical reference for motion correction. The high angular resolution of the diffusion weighting directions improves the robustness of the tensor estimation by increasing the signal-to-noise ratio (SNR) and reducing directional bias. To further increase SNR, scanning was repeated three times for averaging, requiring a total scan time for the DWI protocol of approximately 45 min. DWI data were acquired after the T2-weighted images in the same scanner reference system.

As first step in preprocessing the data, the 3D T1-weighted (MPRAGE; TR = 1300 ms, TI = 650 ms, TE = 3.97 ms, resolution $1.0 \times 1.0 \times 1.0$ mm, flip angle 10°, 2 acquisitions) images were reoriented to the sagittal plane through the anterior and posterior commissures. Upon reorientation, the 3D T2-weighted images (RARE; TR = 2 s, TE = 355 ms, resolution $1.0 \times 1.0 \times 1.0$ mm, flip angle 180°) were coregistered to the reoriented 3D T1-weighted images using rigid-body transformations (Jenkinson et al., 2002), implemented in FSL (2006). The images without diffusion weightings were used to estimate motion correction parameters with the same registration method. The motion correction for the DWI data was combined with the global registration to the T1 anatomy. The gradient direction for each volume was corrected using the rotation parameters. The registered images were interpolated to an isotropic voxel resolution of 1 mm and the three corresponding acquisitions were averaged. Finally, for each voxel, a diffusion tensor was fitted to the DWI data. For presentation purposes, cortical surfaces were rendered on basis of the T1-weighted images by using Freesurfer (Dale et al., 1999).

Definition of the region of interest

Since the lateral premotor cortex cannot be determined on the basis of macroanatomical landmarks, and individual cytoarchitectonic data are not available, we preselected the precentral gyrus (PCG) in each individual, i.e., the anatomical region that is considered to comprise (part of) BA 4 and BA 6 (Brodmann, 1909). The precentral gyrus amounts to the posterior convolution of the frontal lobe, and is bounded in back by the central sulcus and in front by the precentral sulcus. Accordingly, central and precentral sulcus were determined on 1 mm thick axial slices in each individual (MRICron, Rorden et al., 2007). Two-dimensional slices containing these selection markers then entered in an interpolation to generate 3D ROI volumes in the left and in the right hemisphere of all 10 subjects. This selection was further validated by a comparison with the probabilistic microstructural map of BA 6, based on a postmortem analysis of the agranular frontal cortex in ten brains (Geyer, 2004; Eickhoff, 2006). While selecting the PCG may have come at the cost of underestimating the extension of the dorsal PM close to the midline, this choice ensured that we excluded anteriorly adjacent prefrontal tissue from our sample which was not of interest for the present investigation.

The region of interest (ROI) was defined by an experienced neurologist (DYC) on the individual T1-weighted MR images. It encompassed the precentral gyrus bilaterally, bounded by the central, precentral, lateral, and interhemispheric sulci. The ROIs were segmented into white and gray matter compartments thresholding the fractional anisotropy (FA) of the diffusion tensor (white matter: FA>0.1). Each white matter voxel in the ROI that neighboured a gray matter voxel was labeled as seed point for subsequent diffusion tractography.

Diffusion tractographic method

We applied a 3-dimensional extension (Anwander et al., 2007) of the random walk method proposed by Koch et al. (2002). The algorithm was applied to each of the seed voxels. The target space was the whole white matter volume with a resolution of $1.0 \times 1.0 \times 1.0\ mm^3$. The algorithm can be described by a model of randomly moving particles. Imagine a particle in a seed voxel **A**, moving in a random manner from voxel to voxel. The transition probability to a neighbouring voxel depends on the local probability density function (lPDF) based on the local diffusivity profile that is modeled from the DTI measurement. This lPDF is discretised into 26 directions corresponding to neighbouring voxels and yields higher transitional probabilities along directions with high diffusivity, i.e., the presumed fibre directions. Hence, the particle will move with a higher probability along a fibre direction than perpendicular to it. If we perform this "experiment" many times and count how often particles from voxel **A** reach a target voxel **B**, we obtain a relative measure of the probability of tracing a pathway between the two voxels. The random walk is stopped when the particle leaves the white matter volume. The 3-dimensional distribution of the connectivity values of a particular seed voxel with all voxels in the brain is called a *tractogram*. The average tractogram, i.e., the arithmetic mean of connectivity probabilities for each seed point in each volume of interest (VOI), for an entire region we call the *connectivity signature* of this region.

For each elementary transition of the particle, the probability for a movement from the seed voxel m to the target voxel n (the lPDF) is computed as

$$P(m \rightarrow n) = \left(d_{m \rightarrow n,m} \cdot d_{m \rightarrow n,n}\right)^a$$

$P(m \rightarrow n)$: probability for a transition from voxel m to voxel n, $d_{m \rightarrow n,m}$: diffusion coefficient in voxel m for the direction of the connecting line between voxel m and n.

The exponent $a = 7$ is used to focus the probability distribution to main fibre direction and reduce the influence of the transverse diffusion. The value was empirically chosen in such a way that the trajectories of most particles follow the main fibre directions as defined by the lPDF. The transition directions in the local model are limited to the 26 discrete neighbours of the voxel, which is sufficient to produce a smooth distribution of the fibres directions after interpolation of the tensor data to 1 mm voxel size. A total of 100,000 particles were tested for each seed voxel. To compensate for the distance dependent bias, each connectivity value is normalized to the shortest pathway[1] between the seed and the respective target voxel (Anwander et al., 2007). After reducing the dynamic range of the connectivity values by logarithmic transformation, the entire tractogram was scaled to its maximum value. To remove random artefacts, only connectivity values bigger than 0.4 were used for further processing (Anwander et al., 2007).

Cortex parcellation

The idea underlying cortex parcellation is that cortical areas with similar long-range connectivity are combined to one region, which is segregated from neighbouring regions with different connectivity. The connectivity pattern of a cortical voxel is approximated by the tractogram associated to its neighbouring white matter voxel, i.e., the seed points for our diffusion tractography algorithm reside at the gray matter/white matter interface to ensure that the computed tractographic signatures are dominated by long-range connections, within the given resolution. This kind of segregation technique has been termed connectivity-based parcellation accordingly (Johansen-Berg et al., 2004). The general principle of the tractographic and parcellation technique that we applied here is outlined by Anwander et al. (2007).

Functional MRI experiments

Subjects

Two women and two men (29–33 years, mean age 29.8 years) of the 10 subjects of the DWI experiment participated in three functional experiments. Trials of Experiments 1 and 2 were measured within the same experimental session (order counterbalanced between individuals), and those of Experiment 3 in an extra session. In order to enhance signal-to-noise ratio within single subject data while at the same time respecting a maximal scanning time of about 45 min/d and session, participants performed in the first type of session (containing trials of Experiments 1 and 2) three times on three different days. Together with Experiment 3, subjects participated in four sessions on four different days in total.

Logistic limitations ruled out testing all 10 subjects (6 out of 10 students with the DTI data set were no longer available). Note that these limitations do not impose a problem on the interpretation of our data because DTI and fMRI were conducted independently from each other.

fMRI Experiment 1

Within each trial, subjects were presented with sequences of seven stimuli. Trials of the condition TONGUE showed two-syllable pseudo words like LOYO or YALA, whereas trials of the condition HAND showed random numbers from 1 to 4. Participants were instructed to silently say the pseudo word by using only the tongue, or to perform a finger-opponent movement according to the number on the screen (1 = touching thumb with the index finger, 2 = touching thumb with the middle finger, and so on). Each trial started with a 500 ms task cue (TONGUE or HAND) followed by a 200 ms fixation cross and seven stimuli presented consecutively for 1000 ms each with a 1000 ms gap (Fig. 1A). Trial onset asynchrony was 16 s (fix), but within each trial, the task cue was preceded by a variable jitter of 0, 500, 1000, or 1500 ms. 18 trials per condition were presented in a random trial design, resulting in 126 movements per motor effector. Additionally, six empty trials were randomly interspersed.

fMRI Experiment 2

Three experimental conditions of a serial prediction task (Schubotz, 1999) were employed in a random trial design. In each condition, subjects were presented with sequences of twelve abstract geometric stimuli. On each screen, two identical figures appeared on opposite locations of a virtual circle (detailed description of stimuli in Schubotz et al., 2001). Depending on the task cue, participants were required to attend to the order of durations (condition RHYTHM), objects (condition OBJECT), or locations (condition POSITION). The stimulus order was made up by four presentations of a three-element sequence ($4 \times 3 = 12$ stimuli). In half of the trials, the presentation order of picture 11 and 12 was switched with respect to the task relevant stimulus property, resulting in a sequence violation. For example, in the RHY task, a three-element rhythm was presented by picture 1-2-3 lasting 600-300-1500 ms. This rhythm was correctly repeated two further times before picture 11 and 12 switched with respect to their presentation duration, resulting in a new rhythm of 600-1500-300 ms

[1] The "shortest pathway" between seed and target voxel refers to the smallest number of jumps that any one out of the 100,000 test particles has needed to reach the particular target.

(violation of rhythm sequence). For the OBJ task, for instance objects numbered 5-2-7 could be presented three times in orderly succession, but end with sequence 5-7-2 (violation of object sequence). Likewise, items could be presented at positions numbered 8-12-3 three times in succession but at positions 8-3-12 at the end of the same trial (violation of position sequence).

At the end of each trial, subjects were asked to indicate the presence or absence of a sequence violation via button press in a forced-choice response mode (violation = index finger, no violation = middle finger of the right hand). Each trial started with a 600 s task cue (RHY, OBJ, POS), followed by a 400 ms fixation. Then, 12 stimuli were presented for 800 ms each (conditions POSITION and OBJECT) and 300 to 1800 ms each (condition RHYTHM; average stimulus duration 800 ms) without a temporal gap. Trials ended with a question mark, signaling for a 1500 ms phase in which the response was to be delivered, and a 400 ms feedback (correct, incorrect) (Fig. 1B). As in Experiment 1, trial onset asynchrony was 16 s (fix), but within each trial, the task cue was preceded by a variable jitter of 0, 500, 1000, or 1500 ms. 42 trials were presented per condition in a random trial design, in addition to 24 empty trials.

fMRI Experiment 3

Subjects were presented with scenes (movie clips) showing real objects and two hands from the perspective of the observer performing an action. Ten to 20 artifacts or tools from everyday life were loosely arranged on a table. Objects were rearranged and/or exchanged from trial to trial. In condition MANIPULATION, subjects observed a right hand grasping one of the objects followed by a bimanual manipulation of the object in either an action-related (e.g., cutting with scissors) or in a pragmatically meaningless way (e.g., shaking scissors). Subjects were asked to indicate the type of manipulation (button A for meaningful, button B for meaningless manipulation). In condition POINTING, subjects observed the actor's right arm approaching the objects and finally pointing towards one particular object or between two objects. The subjects' task was to distinguish between these cases, pressing response button A for exact pointing, and response button B for between-objects pointing. Each trial started with a 500 ms fixation, followed by 5000 ms movie and a 1000 ms response phase (question mark on the screen); finally, a 500 ms feedback was presented (Fig. 1C). Trial onset asynchrony was 12 s (fix), but within each trial, the fixation was preceded by a

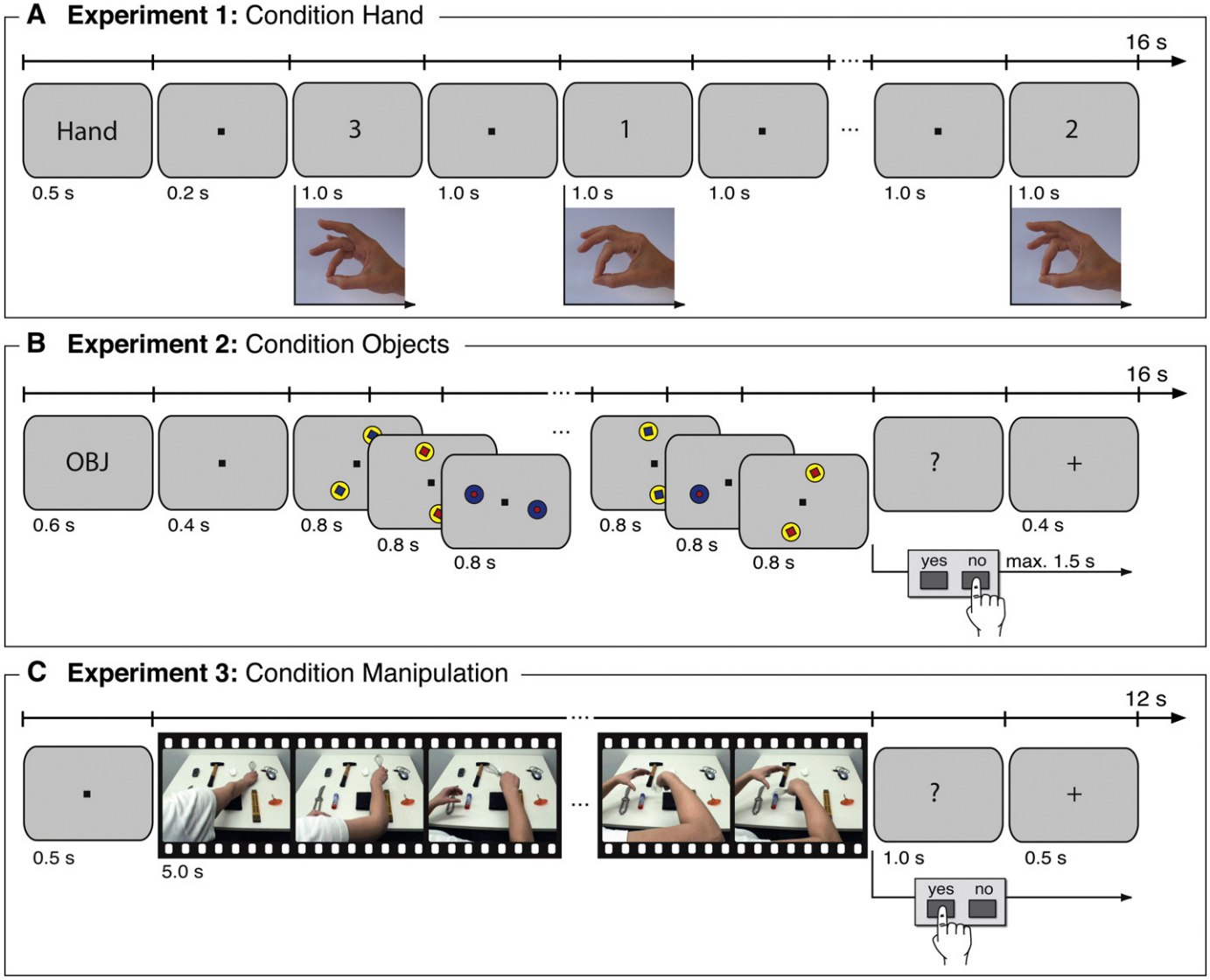

Fig. 1. Illustration of the fMRI paradigms (selected experimental conditions). (A) In Experiment 1, subjects were required to move their tongue or fingers according to visual stimuli. (B) In Experiment 2, a serial prediction task was used which required subjects to attend to the order of durations, objects, or spatial locations. The trial example given in the Figure shows an object prediction trial with a sequential violation (i.e., last two frames are exchanged). Note that in the figure, only two of four sequences are shown and replaced by suspension points. (C) In Experiment 3, short movie clips were presented showing either an object manipulation or a pointing action. Subjects were required to classify manipulations as being action-like or not, and pointing actions to be directed towards an object or between two objects. For further details, see methods.

variable jitter of 0, 500, 1000, or 1500 ms. Sixty trials were presented per condition in a random trial design, in addition to 30 empty trials.

Data acquisition

Participants were supine on the gantry, with two fingers of their right hand positioned over the corresponding response buttons in Experiments 2 and 3. The participants' hands were carefully stabilized, and form-fitting cushions were used to prevent arm, hand, and head motion. To attenuate scanner noise, participants were provided with earplugs. Imaging was performed on a 3T scanner (Siemens TRIO, Erlangen) equipped with the standard birdcage head coil. For registration purposes, a set of two-dimensional anatomical images were acquired for each participant immediately before the functional imaging. T1-weighted modified driven equilibrium fourier transform (MDEFT) images (256×256 pixel matrix) were obtained with a non-slice-selective inversion pulse followed by a single excitation of each slice. Anatomical images were positioned parallel to the bicommissural plane (anterior commissure–posterior commissure). Functional data were acquired from 18 axial slices (thickness 4 mm; gap 25%) by using a single-shot gradient echo echo-planar imaging (EPI) sequence (echo time 30 ms; pixel matrix 64×64; flip angle 90°; field of view 192 mm). During each trial, eight (Experiments 1 and 2) and six volumes (Experiment 3) were obtained at a rate of 2 s per volume, resulting in a total of 480 (Experiment 1), 1200 (Experiment 2), and 900 (Experiment 3) functional images for each participant. Due to the repetition protocol of experimental sessions 1 and 2, the total number of volumes was 1440 for Experiment 1 and 3600 for Experiment 2.

Functional imaging data analysis

The fMRI data processing was performed by using the software package LIPSIA (Lohmann et al., 2001). Functional data were motion-corrected offline with the Siemens motion correction protocol (Siemens). To correct for the temporal offset between the slices acquired in one scan, a cubic-spline interpolation was applied. A temporal high-pass filter with cutoff frequencies of 1/120 Hz (Experiment 1 and 2) and 1/90 Hz (Experiment 3) were used for baseline correction of the signal; since individual data were analyzed, no spatial Gaussian filtering was applied. To align the functional slices with a 3D stereotactic coordinate reference system, a rigid linear registration with six degrees of freedom (three rotational and three translational) was performed. The rotational and translational parameters were acquired on the basis of the MDEFT and EPI-T1 slices to achieve an optimal match between these slices and the individual 3D reference data set. This 3D reference data set was acquired for each subject during a previous scanning session. The MDEFT volume data set with 160 slices and 1-mm slice thickness was standardized to the Talairach stereotactic space (Talairach & Tournoux, 1988). The rotational and translational parameters were then used to transform the functional slices by using trilinear interpolation so that the resulting functional slices were aligned with the stereotactic coordinate system.

The statistical evaluation was based on a least-squares estimation by using the general linear model for serially autocorrelated observations (Friston, 1994; Friston et al., 1995a,b; Worsley and Friston, 1995). The design matrix was generated with a boxcar function (Experiment 1 and 2) and a gamma function (Experiment 3), convolved with a hemodynamic response function including a delay of 6 s. The analyzed epoch comprised the time in which subjects were presented with stimuli (including corresponding movements in Experiment 1), i.e., phases of 14 s (Experiment 1), 9.6 s (Experiment 2), and 5 s (Experiment 3). The model equation, including the observation data, the design matrix, and the error term, was convolved with a Gaussian kernel of dispersion of 4 s full width at half maximum.

For the analysis of individual data sets, required for determining structure-function-correspondence, z-maps of the differences between the specified conditions were calculated for each subject. The following contrasts were calculated: (1.a) tongue>fingers and (1.b) fingers>tongue (Experiment 1); (2.a) RHY>OBJ & POS, (2.b) OBJ>RHY & POS, (2.c) POS>RHY & OBJ (Experiment 2); (3.a) grasping>pointing and (3.b) pointing>grasping (Experiment 3). For the analysis of group effects which was merely performed for descriptive purposes (cf. Fig. 6), contrast images of the differences between the specified conditions were calculated for each subject (same contrasts as in the single subject data analysis). Group analyses (random-effects model) based on the contrast images were subsequently performed. The individual contrast images were then entered into a second-level random effects analysis (one-sample *t* test). Subsequently, *t* values were transformed into Z scores. To protect against false-positive activations, only regions with a *Z* score>3.09 ($P<0.001$ uncorrected) and with a volume>135 mm^3 (5 contiguous voxels) were considered (Forman et al., 1995).

Assessment of structure-function correspondence

To assess the degree of correspondence between the individual functional activation patterns (revealed by fMRI) and the anatomical areas (revealed from cortex parcellation), we computed the relative overlap (OL%):

$$R_{ij} = \frac{N_{ij}^{fMRI+DTI}}{\sqrt{N_i^{fMRI}} \cdot \sqrt{N_j^{DTI}}} \quad (1)$$

$N_{ij}^{DTI\ +\ fMRI}$ denotes the number of superficial gray matter voxels that belong to both the functional activation pattern *i* and the anatomical area *j*, N_i^{fMRI} is the number of voxels in the functional activation pattern i and N_j^{DTI} is the number of voxels in the anatomical area *j*. In each hemisphere, we computed all relative overlaps according to equation (1) between the 14 functional activation patterns (7 contrasts in 2 hemispheres: tongue>fingers, fingers>tongue, rhythm>object and position, object>rhythm and position, position>rhythm and object, grasping>pointing, pointing>grasping) and the 4 anatomical areas.

In order to statistically test whether there is a significant correlation between the activation patterns and anatomical areas across individuals, we applied a bootstrap approach by first computing two different distributions for the relative overlaps. In the random match condition relative overlaps between activation patterns of any subject and cortical areas of any other subject (which may also be the same) were included into the distribution. In the correct match condition the distribution only comprises relative overlap values within subject.

If indeed the particular cortex parcellation in a particular subject predicts functional activation patterns in the same subject better than the functional activation in any other subject, the two distributions should be different. More specifically, one would predict for the correct match condition a higher incidence of low relative overlaps (if the particular anatomical area does not support the particular function) and high relative overlaps (if the anatomical area is part of the neuronal substrate of the respective function), while intermediate values are less frequent.

Quantification of interindividual parcellation reproducibility

In order to quantify the parcellation reproducibility over subjects, the following strategy was employed. For each hemisphere, the relative overlaps between all pairs of subject–area combinations were calculated. Then, these values were averaged over subjects. The resulting values quantify the mean relative overlap between any pair of areas in different subjects.

Results

Cortex parcellation

The PCG could be consistently divided into two areas in both hemispheres for all 10 subjects: a dorsal area (PCGd) and a ventral area (PCGv) (Fig. 2). On the convexity of the PCG, the average Talairach *z*

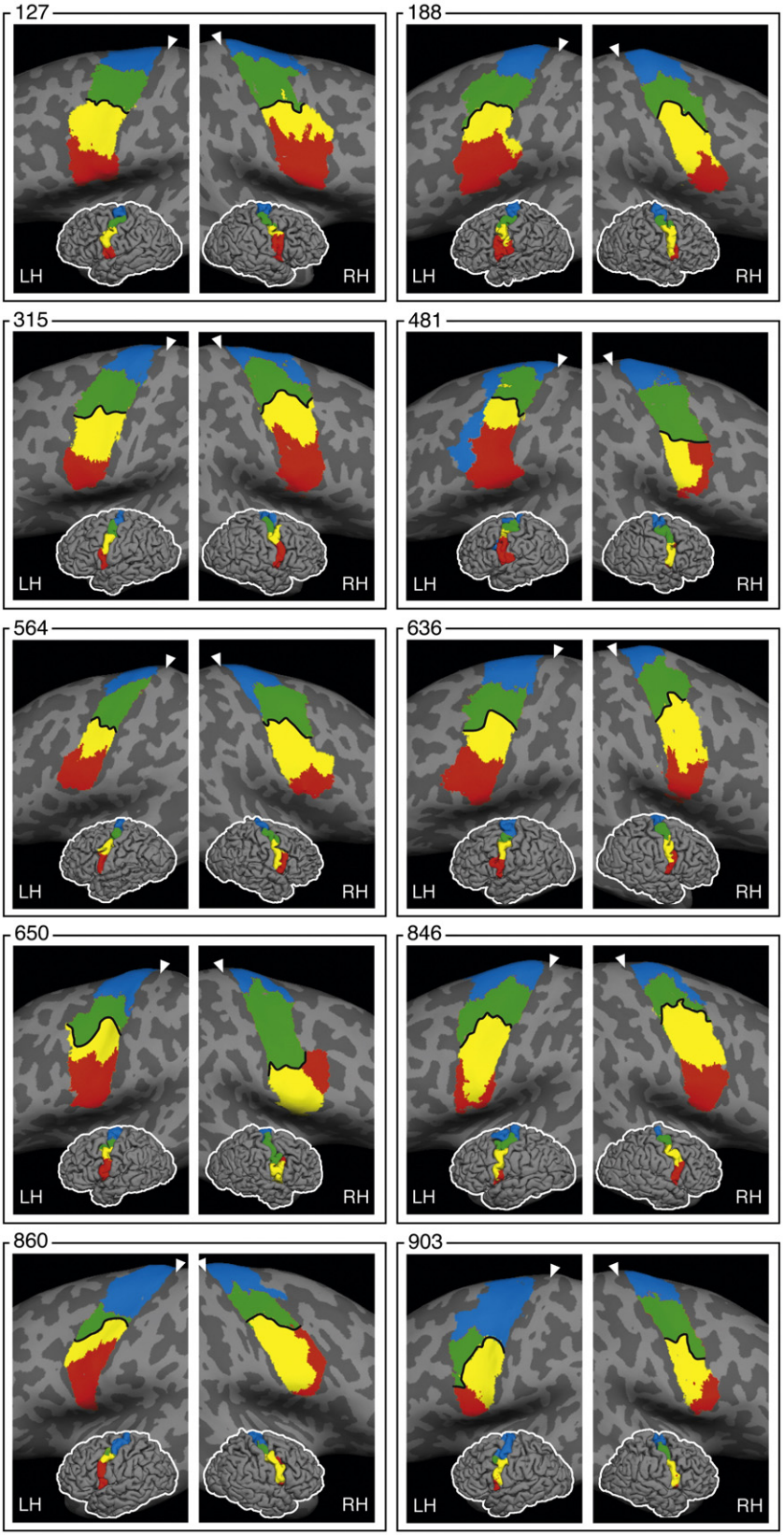

Fig. 2. Connectivity-based parcellation of the PCG. Results of parcellating the left and the right hemisphere for all 10 subjects indicate that the PCG is divided into a dorsal (area PCGd) and a ventral (area PCGv) area in both hemispheres. Further subdivisions yielded consistent parcellations of four clusters, resulting in a superior (blue) and an inferior (green) area of PCGd as well as in a superior (yellow) and an inferior (red) area of PCGv. Arrows indicate the central sulcus in each hemisphere.

coordinate of the border between ventral and dorsal areas was 49 (95% confidence interval: 47 to 51) in the left and 52 (95% confidence interval: 48 to 56) in the right hemisphere. Visual inspection of the connectivity signatures (i.e., the average diffusion tractogram, cf. Anwander et al., 2007) of the dorsal area indicated strong connection probabilities into the descending corticofugal (pyramidal) tracts, to adjacent postcentral areas, to the superior parietal lobule, and to the posteriormost portion (foot region) of the middle frontal gyrus. For the ventral part, connection probabilities were found to the middle and the inferior frontal gyri, to superior and inferior parietal areas, and to temporal regions.

However, an equivalently consistent parcellation across subjects showed up at four clusters (Fig. 2). Both the dorsal area and the ventral area were subdivided again into a superior–caudal and an inferior–rostral area (hereafter superior PCGd, inferior PCGd, superior PCGv, inferior PCGv), respectively.

The connectivity signatures of the different regions showed strong pyramidal connection probabilities for superior PCGd, and a more diverse pattern dominated by connections with the caudal dorsolateral prefrontal cortex for inferior PCGd. Across subjects, there were consistent connections (cf. Fig. 3) into the directly adjacent postcentral region (BA 5) for superior PCGd (left: 9 of 10 subjects; right: 8) but

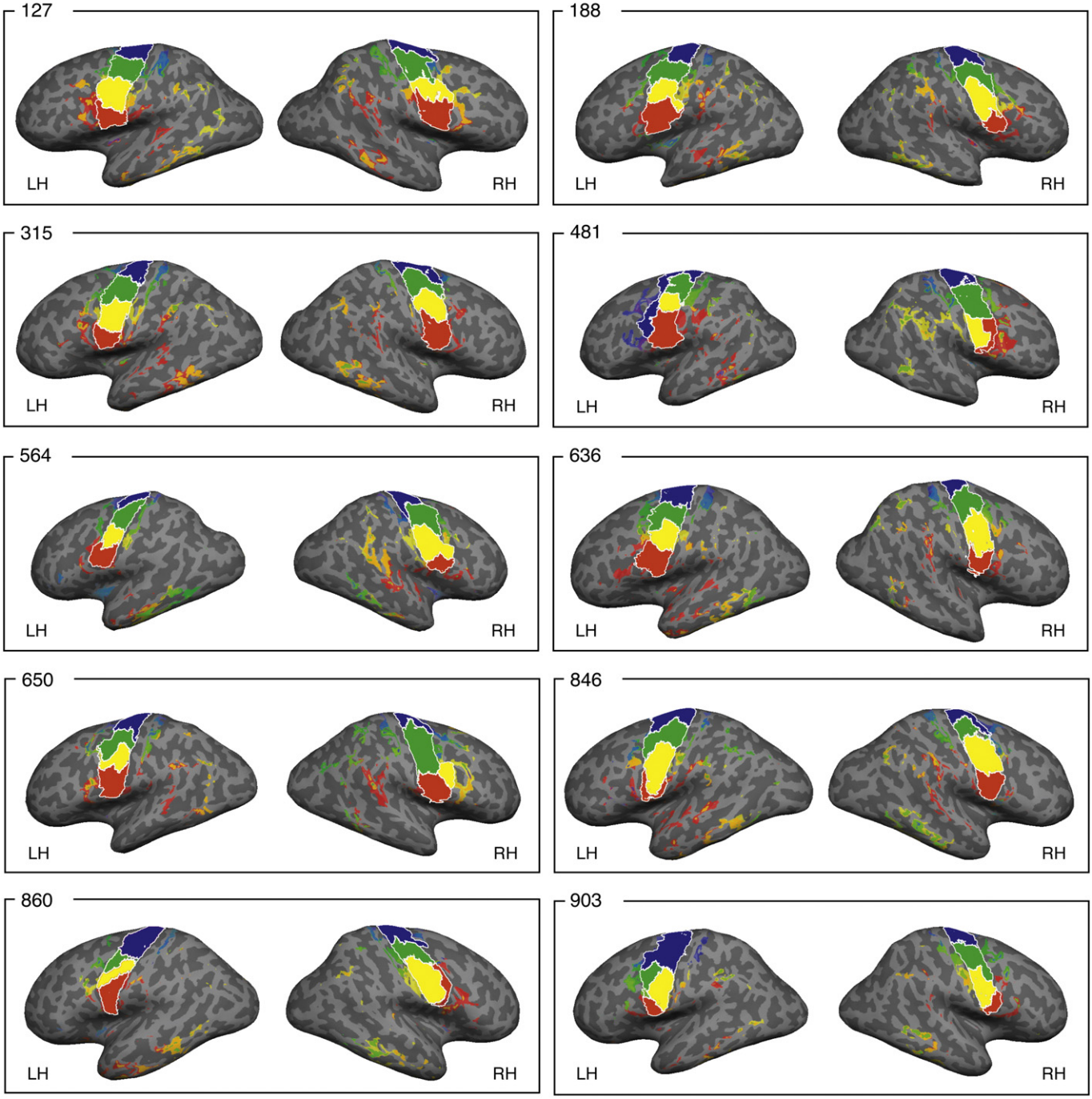

Fig. 3. Tractographic target sites for each of the four parcellated PCG fields in each of the ten subjects. Tractography was started at the white matter–gray matter interface in any point for each individual parcellated field. The endings of tractograms at a cortical location (tractographic target sites) are depicted color-coded (cf. Fig. 2) for each field. The pattern of such targets indicates the characteristic anatomical connectivity of the particular field.

insignificant prefrontal targets; for inferior PCGd, consistent connections were found in directly adjacent postcentral area reaching into the superior parietal lobule (BA 5 and BA 7; left: 7 of 10 subjects; right: 10) and in the posterior portion of the middle frontal gyrus (BA 8; left: 7 of 10 subjects; right: 7).

The two ventral regions showed connections to the parietal and the temporal lobe. For superior PCGv, the interindividually most consistent connections across subjects were found around the anterior intraparietal sulcus (BA 7/39; left: 7 of 10 subjects; right: 6). In addition, subjects showed prefrontal connection probabilities into lateral BA 9 and/or BA 44 (left: 5 of 10 subjects; right: 4) as well as into different temporal regions (left: 8 of 10 subjects; right: 6). In contrast, inferior PCGv showed parietal connections mostly around supramarginal gyrus and angular gyrus (BA 39/40; left: 5 of 10 subjects; right: 6), but no connection probabilities with the superior parietal lobule (BA 7). Also for this area, very consistent connections were found into BA 44 (left: 9 of 10 subjects; right: 10) and into temporal regions (left: 10 of 10 subjects; right: 7); some subjects also showed prefrontal connections with the posterior portions of the upper bank of the inferior frontal sulcus (left: 6 of 10 subjects; right: 5). Thus, while both ventral areas showed parietal and temporal connection probabilities, their connection patterns were consistently different across subjects.

As to the quantification of the parcellation reproducibility over subjects, the mean relative overlaps between any pair of areas in different subjects are displayed in matrix form in the right panel of Fig. 4. If the resulting matrices (one per hemisphere) are strongly diagonal, this means that corresponding fields agree much better between different subjects than noncorresponding ones, i.e., the parcellations are similar between subjects. As a result, the values were much bigger in the main diagonals, i.e., between the same areas across different subjects. Some overlap can also be observed between adjacent areas (so-called secondary diagonals), especially between the two ventral areas in the right hemisphere where the parcellation is in two subjects rostro–caudal rather than ventral–dorsal. The population maps in the left part of Fig. 4 illustrate the variability of the areas.

Functional MRI data

The motor localizer tasks (Experiment 1) yielded clearly distinguishable activations located in the caudal precentral and in the postcentral gyrus for both finger and tongue movements (Fig. 5A). Finger movements activated the well-known region of the inverted omega-shape on the PCG (Yousry et al., 1997) whereas tongue movements elicited activations in a more ventral region close to the one reported by Fox and colleagues (2001). Fox and colleagues report the left mouth area at Talairach coordinates x/y/z of −46/−8/40 and the right at 52/−8/38; in comparison, the average location of activation was −50/−9/36 and 55/−6/42 in our subjects (for comparison, average location of the right finger movements was −29/−17/60).

As expected on the basis of previous results, Experiment 2 replicated that rhythmic, object-based and spatial sequence tasks activate different portions of the lateral premotor cortex to different extents (Fig. 5B). Note that these differences, based on direct contrasts between experimental conditions, reflect relative variations of the BOLD response rather than absolute differences. In contrast to the object and the spatial task, rhythmic sequences corresponded to activation in the right inferiormost ventral premotor cortex; object sequences caused highest activation in the left superior ventral premotor cortex; spatial sequences led to most pronounced signal changes in the dorsal premotor cortex in both hemispheres. Maximally activated areas were, on average, (43/10/9) for rhythm sequences, (−41/−3/27) for object sequences, and (−29/−5/66) and (28/−8/58) for spatial sequences.

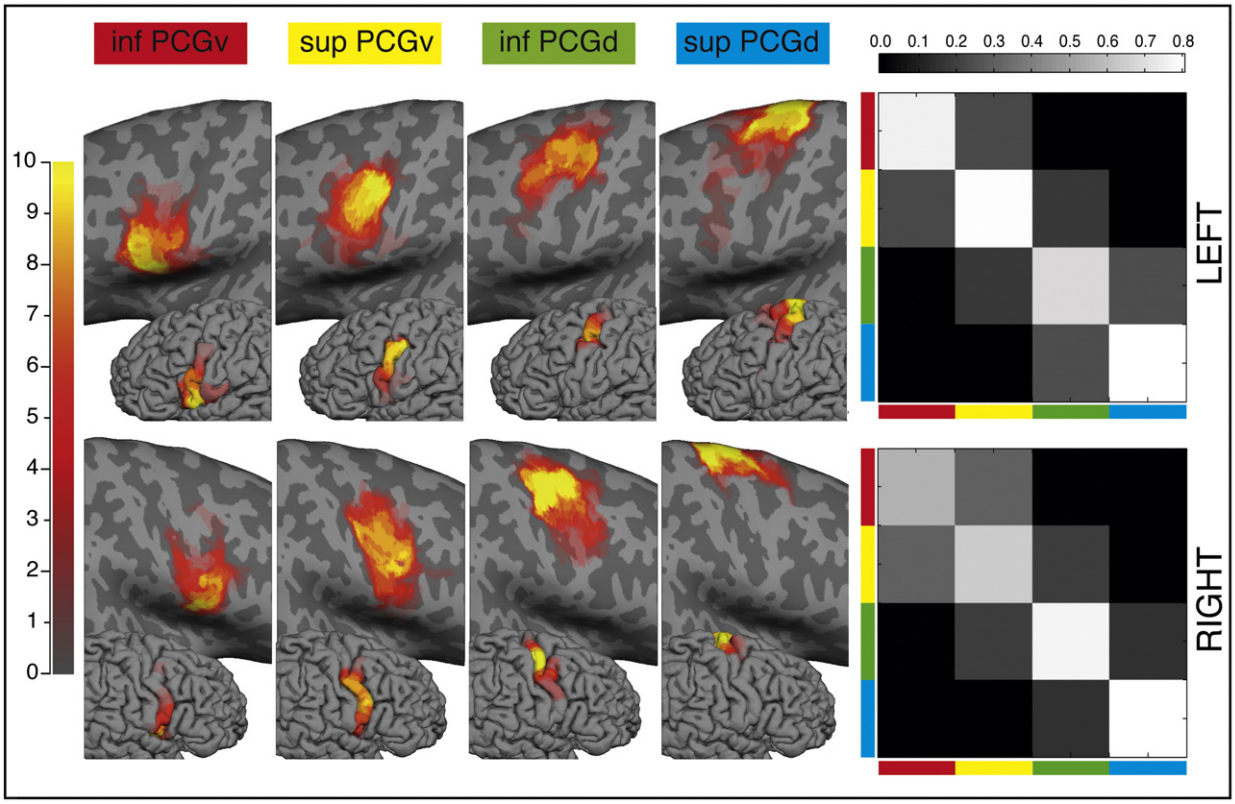

Fig. 4. Relative overlap (scale ranging from 0 to 10 subjects) of each individual area in the left (upper panel) and right (lower panel) hemisphere, respectively. Population maps are plotted onto the inflated cortex as well as onto the pial surface (smaller insets). Matrices on the right side depict a quantification the mean relative overlap between areas.

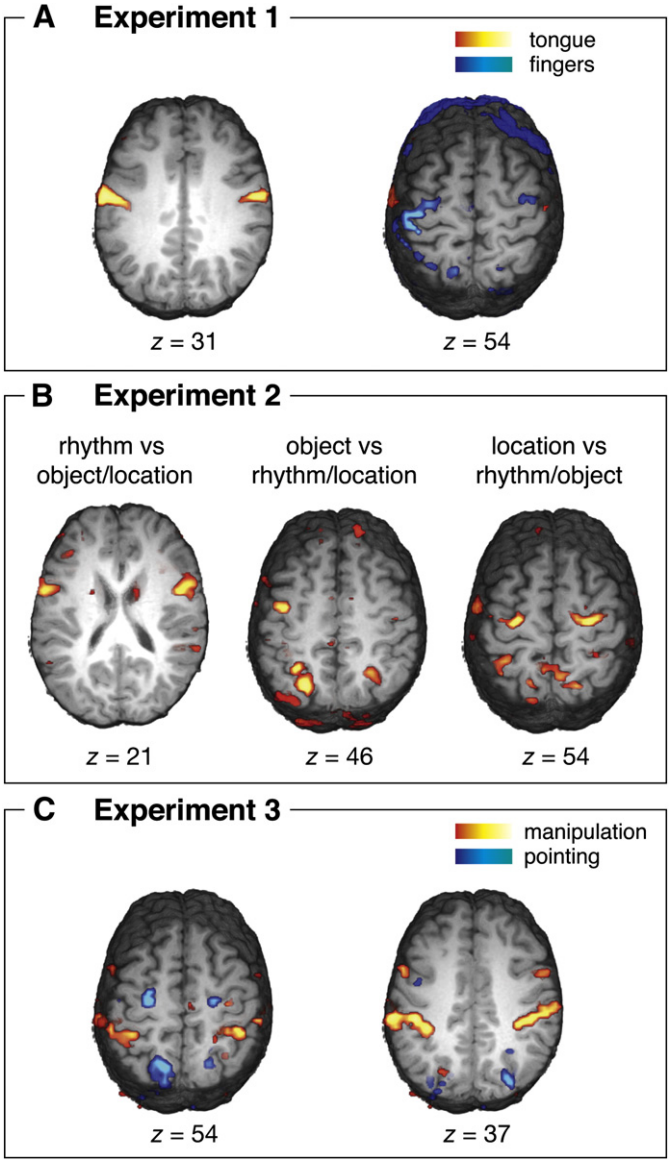

Fig. 5. Representative fMRI data of one individual subject. Z maps show maximal activated voxels (Z score>3.09, P<0.001 uncorrected, volume>135 mm^3) for direct task contrasts from Experiment 1 (tongue vs. hand, hand vs. tongue), Experiment 2 (rhythm vs. objects and positions, objects vs. rhythm and positions, positions vs. rhythm and objects), and Experiment 3 (observation of grasping/manipulation vs. observation of pointing, observation of pointing vs. observation of grasping/manipulation).

In Experiment 3, watching movies of object grasping/manipulation as compared to observing pointing movements directed at or between objects was particularly correlated with activations in the ventral PCG. The opposite contrast revealed specific activation in dorsal PCG, slightly stronger on the left side (Fig. 5C).

Systematic comparison between fMRI findings and cortex parcellation

None of the fMRI contrasts we reported revealed activation restricted to only one single PCG field. However, activation was distributed differently depending on the task contrast (Fig. 6). Since there are no standards of how to compare diffusion-based cortical parcellation with fMRI data, we computed for each subject and hemisphere the *relative overlap* between each pair of cortex parcellation area and the cortex area activated in a certain experimental contrast. The relative overlap was then subjected to a bootstrap approach (see Methods).

As to the relative overlaps between activation patterns and cortical areas, we found a clear difference between the random match distribution and the correct match distribution, as depicted by the normalized histograms in Fig. 7. In detail (as presented in Fig. 6), tongue movements (Experiment 1) exposed significant activations nearly exclusively in the ventral fields (~91% of relative overlap, hereafter ~$91\%_{OL}$) as compared to hand movements (PCGv>PCGd TONGUE: $t(7)=14.631$, $p<0.001$, according to a Students' t test), whereas for hand movements, the major portion of activation (~$66\%_{OL}$) was recorded in the dorsal PCG fields (marginal effect: PCGd>PCGv HAND: $t(7)=2.09$, $p<0.075$). For Experiment 2, activation was almost restricted to the ventral fields for rhythmic as compared to object and spatial sequences (PCGv >PCGd RHYTHM: $t(7)=13.652$, $p<0.001$). There was a clear asymmetry indicating rhythm activity to be more pronounced in the inferior (~$61\%_{OL}$) as compared to the superior (~$29\%_{OL}$) PCGv (inferior PCGv>superior PCGd RHYTHM: $t(7)=2.574$, $p=0.037$). Similarly, object sequences showed particularly ventral PCG activation (PCGv>PCGd OBJECT: $t(7)=2.551$, $p=0.0381$) but with a (non significant) tendency towards the opposite distribution (~$31\%_{OL}$ inferior vs. ~$43\%_{OL}$ superior); however, more than a further $22\%_{OL}$ of the voxels activated in this contrast fell into inferior PCGd. In contrast, spatial sequences elicited activations particularly in the dorsal fields (~$40\%_{OL}$ inferior, ~$18\%_{OL}$ superior) and showed less activity in the ventral areas (~$28\%_{OL}$ superior, ~$14\%_{OL}$ inferior), but the statistical effects were only marginal (PCGd>PCGv POSITION: $t(7)=1.954$, $p=0.0916$). In Experiment 3, finally, observation of grasping/manipulation of objects showed again a clear preference for ventral areas (~$82\%_{OL}$, PCGv>PCGd MANIPULATION: $t(7)=4.848$, $p=0.002$), with a particular dominance of the inferior PCGv (~$65\%_{OL}$; inferior PCGv>superior PCGd MANIPULATION: $t(7)=3.835$, $p=0.006$). For pointing observation, the opposite pattern was found with more than $65\%_{OL}$ in the dorsal fields and the rest of it in the superior PCGv; no normalized overlap was registered in the inferior PCGv for this condition.

Discussion

The present study used both diffusion tractography and fMRI to investigate the structural and functional properties of the human precentral gyrus (PCG) in the same subjects. As major results on structure, our data suggest a ventral and a dorsal PCG field that could be further segregated into superior and inferior parts, respectively, resulting in four PCG fields altogether. With respect to functional properties, we report preliminary evidence for cortex parcellation to be paralleled by functional profiles in three fMRI studies.

Four distinguishable subareas in PCG

On the basis of functional imaging studies, Rizzolatti and colleagues (2002) have proposed that human dorsal premotor cortex is located superiorly and ventral premotor cortex inferiorly to about z = 51 (pial surface) of Talairach space. This view is well corroborated

Fig. 6. Comparison between functional activations (fMRI data) and cortex parcellation of the PCG. The left panel shows individual fMRI data of both hemispheres of four subjects, together with the outlines of the diffusion-based PCG fields (white lines) overlaid to the corresponding inflated individual anatomies. Significantly activated voxels were color-coded for each contrast (see legends) and then collapsed into one view per hemisphere and experiment. The right panel shows the corresponding relative overlaps (OL%) between connectivity-based parcellation and functional activations per experimental contrast and averaged across both hemispheres of all subjects (group data). Colors (cf. Figs. 3 and 4) indicate the relative overlap between significantly activated voxels and the inferior ventral (yellow), superior ventral (red), inferior dorsal (green), and superior dorsal (blue) PCG field as determined by cortex parcellation.

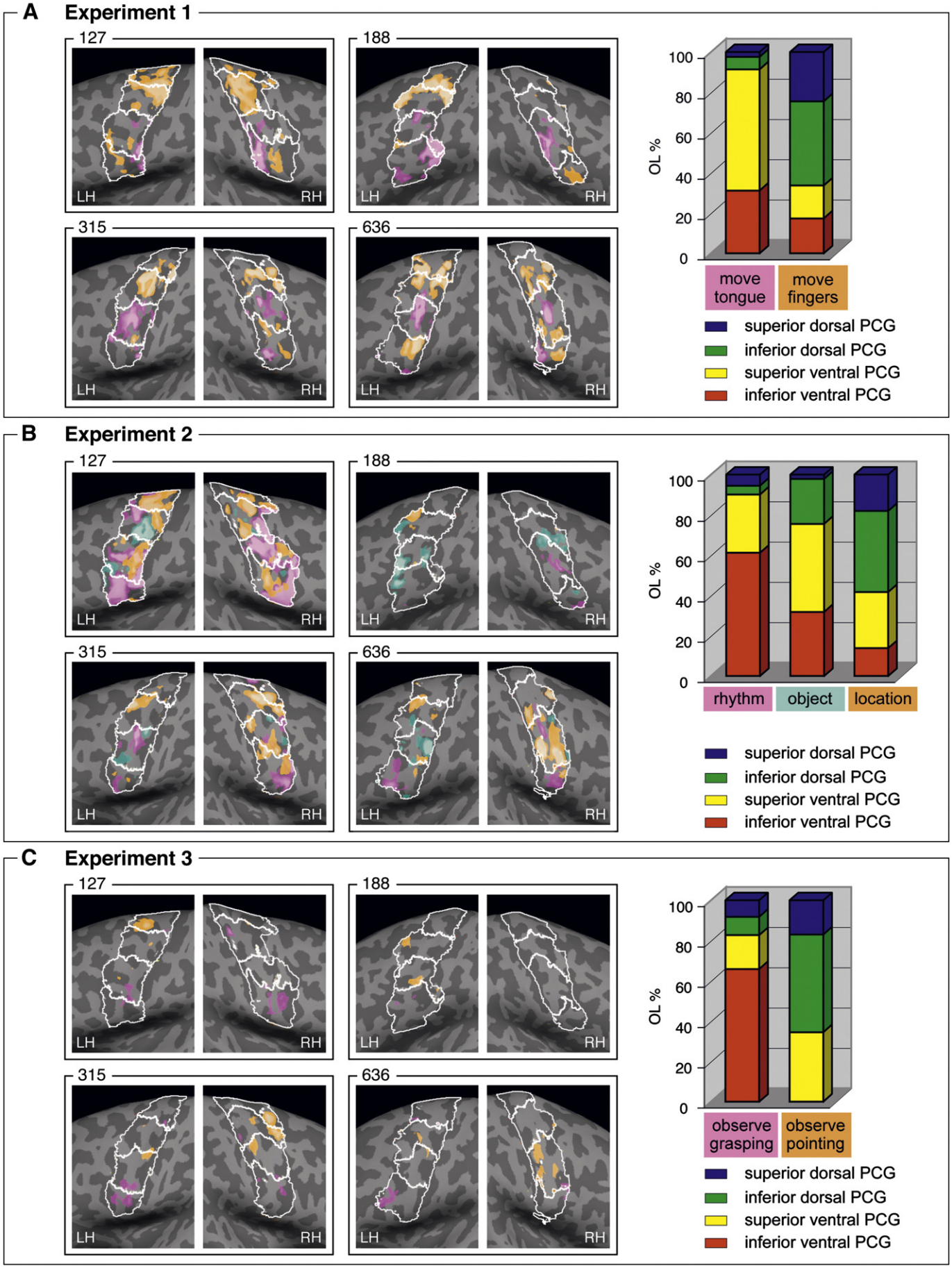
A
Experiment 1
127
188
315
636
LH
RH
OL %
100
80
60
40
20
0
move tongue
move fingers
superior dorsal PCG
inferior dorsal PCG
superior ventral PCG
inferior ventral PCG
B
Experiment 2
rhythm
object
location
C
Experiment 3
observe grasping
observe pointing

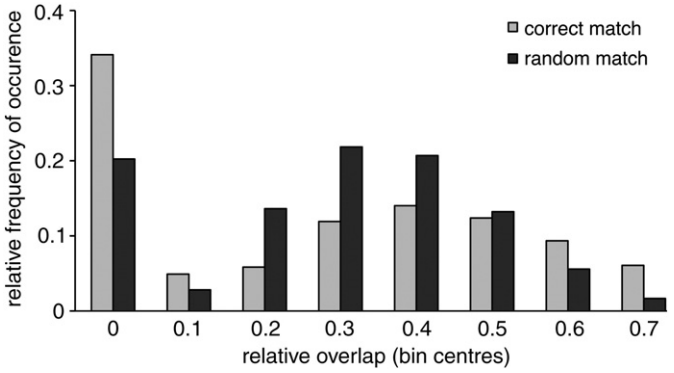

Fig. 7. Normalized histograms of relative overlaps (OL%) between each pair of cortex parcellation areas and functional activation patterns from the fMRI experiments, for the correct match and random match conditions (after square root transformation). If a particular cortex parcellation in a particular subject predicts functional activation patterns in the same subject better than the functional activation in any other subject, the two distributions should be different, and one would predict for the correct match condition a higher incidence of low relative overlaps and high relative overlaps, while intermediate values are less frequent. Clearly, for the correct match condition, the pattern is more binary, with both very low and very high values being more frequent. For details of calculation of OL%, please refer to "Assessment of structure–function correspondence" in the Materials and methods section.

by our findings, as we could separate two more ventral fields from two more dorsal fields at a Talairach level of about z = 49 (left) and 52 (right) at the pial surface.

On the basis of cytoarchitecture, motor representations, sulcal ontogeny, and the putative macroanatomical location of the human frontal eye field, homologies between macaque and human ventral and dorsal premotor cortex have been proposed (Rizzolatti et al., 1998). Accordingly, macaque areas F2 and F7 correspond to the superior part area 6aα and the area 6aβ of Vogt and Vogt (1919), respectively, whereas the inferior part of Vogts' area 6aα and BA 44 (Brodmann 1909) correspond to areas F4 and F5, respectively. That means, however, that among lateral premotor fields only F2 and F4 fall into PCG, whereas both F5 and F7 lie in anteriorly adjacent regions, namely in the opercular part of the inferior frontal gyrus and in the caudal portion of the superior frontal gyrus, respectively. While our findings support a ventral–dorsal border exactly where proposed by Rizzolatti and coworkers (2002), they reflect more than two, namely four, fields within the PCG with typical premotor connectivity. For instance, our inferior dorsal PCG-field exposed prefrontal connection probabilities, which points to a homolog of F7 rather than F2 (which receives prefrontal input from 8B and 46d). Moreover, two fields made up the ventral PCG, which is in line with two ventral premotor fields in the macaque (F4 and F5). An alternative explanation would be that two subareas make up F4, which however has not yet been reported. Together, our findings point to four distinguishable premotor subareas in the PCG.

Despite of some advances to validate diffusion tractography results by autoradiographic tracer techniques in the macaque (Schmahmann et al., 2007), cortex parcellation as inferred by DWI in the human brain and projection areas as revealed by histologic tracer studies in the macaque brain cannot be directly compared. Thus, speculations about putative homologies as suggested by connectivity differences between premotor subregions have to be handled with great caution. For the dorsal fields we identified profiles of connections to primary motor, prefrontal, and parietal areas (Geyer et al., 2000; Rizzolatti & Luppino, 2001; Marconi et al., 2001; cf. Husain & Nachev, 2007) are in line with the suggestion that the superior PCGd could roughly correspond to F2 in the macaque, and inferior PCGd to F7. For the ventral fields, subtle but consistent differences between connectivity signatures of our superior and inferior PCGv may justify the speculation that these regions could correspond to F4 (Colby et al., 1993; Duhamel et al., 1997a,b; cf. Bremmer et al., 2001) and F5 (Godschalk et al., 1984; Matelli et al., 1986; cf. Caspers et al., 2006) of the macaque, respectively. Against the background of the macaque literature, temporal connectivity of our ventral PCG fields have to be considered to reflect indirect rather than direct connections (Luppino et al., 1999; Maioli et al., 1998) via parietal (Rozzi et al., 2006; for literature review, see Keysers & Perrett, 2004) or primary motor cortex (Simonyan & Jürgens, 2002, 2005).

Functional data in relation to cortex parcellation

Extrinsic (parietal and prefrontal) connections differ among premotor subregions in the macaque brain and support their functional differentiation. Following this rationale, we hypothesized cortex parcellations of the PCG to reflect the distribution of BOLD activation assessed in different experimental tasks (Experiments 1, 2, and 3). Note however that differences of extrinsic connections in macaque premotor cortex are clearly limited and reflect differently weighted connectivity rather than absolutely different ones. Also, recent findings from DWI data in humans suggest that the projections from dominant fibre pathways can be quite variable; a prominent example with respect to our results is provided by language-related pathways indicating a noticeably variability in the ventral premotor and adjacent prefrontal region (Rilling et al., 2008., Friederici, 2009).

As to the variable but still very consistent findings on structural subregions in PCG, we think that the ventral premotor cortex is indeed a phylogenetically quite variable structure, which surfaces here in two interindividually different variants: a (less frequent) rostro–caudal organisation (cf. Fig. 2, right hemispheres of subjects no. 481, 650, and 860) and a (more frequent) ventro–dorsal one. In contrast, methodological shortcomings or problems, e.g., due to misalignment, head-motion, imaging artefacts, or scanner setting, would rather result in inconsistent findings across all subjects, and presumably with additional inconsistencies between hemispheres as well. Moreover, the data quality was carefully examined and turned out to be comparable between all subjects.

As expected against this background, individual data sets showed extensive and spreading premotor activation clusters. In order to assess which of the PCG fields contribute more to one experimental condition as compared to another, we focused on direct task contrasts. Hence, we analyzed a weighting profile for the PCG fields in different functional tasks. Moreover, we used a bootstrap approach in order to show that there is a specific assignment of fMRI activations and cortical parcellation.

Experiment 1 served as a localizer study for major primary motor and premotor areas on the lateral convexity, i.e., tongue and fingers. The somatotopical maps of the lateral premotor cortex lie in rough correspondence to those in the primary motor cortex but expose a considerable and ventrally even increasing overlap. There is a forelimb and hindlimb representation in PMd, and an orofacial and forelimb representation within PMv. More specifically, both areas F4 and F5 are organized somatotopically, with arm movements represented dorsally and orofacial movements ventrally. They differ in that distal arm movements (i.e., those of the hand and fingers) are mainly represented in F5, and proximal arm movements in F4 (for a discussion, see Geyer et al., 2000). In F2, leg movements are represented dorsally and (proximal and distal) arm movements ventrally; ventral F7 has a representation of arm movements as well.

We found tongue movements to elicit activations in the inferior ventral and in the superior ventral PCG (~91%), possibly corresponding to F5 and F4, respectively, i.e., those premotor areas, which have an orofacial representation in the macaque. Compared to tongue movements, hand (finger) movements elicited mainly activations in the dorsal PCG (~66%). In monkey dorsal premotor cortex, both subareas F2 and F7 are engaged in arm movements, but only F2 in distal ones, i.e., those which were relevant in our present study. However, F7 is suggested in conditional movement selection and

visual localization of stimuli in space as a prerequisite for reaching movements (Rizzolatti et al., 1998). It hence could be plausible that finger-thumb opposition under abstract (numerical) visual cueing triggered also activation in the F7 homologue. Together, we take the activation pattern induced by tongue and finger movements to be reconcilable with the rough premotor somatotopy reported in the macaque monkey.

Experiment 2 followed the rationale of a series of fMRI studies that investigated the role of the premotor areas in the processing of serial order (Schubotz & von Cramon, 2003; Schubotz, 2004). Findings replicated the typical and robust activation BOLD response pattern, with rhythmic, object-based and spatial sequence tasks activating lateral premotor fields in a ventral-to-dorsal succession. The HAPEM framework (Schubotz, 2007) explains these findings by a repertoire of styles of transformations, primarily coded in PM, that can be exploited for both action and perception. Accordingly, the prediction of an event that is structured with regard to a property P engages the subarea of the lateral premotor cortex that is best adapted to specify its motor output in terms of P. For instance, a spatially defined event (e.g., a rotation) will be simulated using the premotor–parietal loop for reaching because an arm action plan amounts to the expectation of a sequence of mostly spatially defined perceptions. The same mapping logic holds for other pairings as well, connecting object-defined events to the grasping circuit and pitch or rhythm-defined events to the vocal and articulatory circuit. This account suggests that merely a subset of sensorimotor neurons in the areas controlling such actions is exploited in a rudimentary simulation mode. This simulation suffices to predict some of the relevant dynamics of the observed event, but it cannot serve as an exhaustive event description (for detailed explanation of the framework see Schubotz, 2007).

Comparing fMRI data with cortex parcellation, the present study revealed that the four PCG fields showed not absolute but rather relative differences with respect to the activation corresponding to sequence tasks. Thus, the majority of significantly activated voxels during the rhythmic sequence task fell within the inferior PCGv (~61%), whereas those of the object-based sequence task were rather distributed among both inferior (~31%) and superior PCGv (~43%) and those of the spatial sequence task among both PCGd fields (~40% and ~18% for inferior and superior, respectively).

Experiment 3, finally, required subjects to deal with observed actions, either with a focus on grasping/manipulation, or with a focus on pointing. Since the attentive analysis of observed actions has been reported to rely on those premotor areas which are also engaged in the production of the very same actions (for a review, see Rizzolatti & Craighero, 2004), we expected premotor areas for distal arm movements and those for proximal arm movements to be detected in the respective direct condition contrasts. Specifically, the former should roughly correspond to the human homologue of F5, the latter to the human homologues of F2, F4, and F7 (for a literature overview, see Geyer et al., 2000). In line with these considerations, we found the observation of grasping/manipulation to especially activate voxels of the inferior PCGv (~65%); remaining voxels fell either in superior PCGv (~17%) or in the PCGd. Pointing observation, as expected, particularly activated the superior PCGv (~35%) and the inferior PCGd (~48%), which could reflect, according to our present interpretation, the human homologues of F4 and F7, respectively, and some voxels (~17%) in the superior PCGd. Hence, the pattern of activation was comparable between pointing observation and the spatial sequence task from Experiment 2, as expected (cf. Schubotz, 2007).

Overall, functional data from three fMRI experiments were largely consistent with the interpretation of the cortex parcellation of four subregions in the PCG. This finding parallels a methodologically similar approach to separate two subregions of the supplementary motor area (SMA proper vs. pre-SMA, Johansen-Berg et al., 2004). However, our results also showed that functional activations were not sharply restricted to the connectivity-based fields. This difference may be due to the fact that the contributions of the subregions of the PCG are differently weighted for different functional requirements rather than exclusively engaged in only the one or the other function or task. To give an example for the cognitive domain, even when only a rhythmic sequence is to be processed, the task-relevant information is supplied via a stimulus that necessarily has object and spatial properties as well. These properties may be considered even when task-irrelevant, particularly because in ecological environments, dynamic changes of a stimulus property typically coevolves with changes of (some of) its other properties as well. For instance, when we have to predict the trajectory of a ball, parameters of its speed, location, and surface will alter concurrently. Turning to an example for the motor domain, movements of the fingers frequently require or entail concurrent movement of the wrist, and sometimes even those of the elbow and the shoulder. Across all motor fields, limbs are represented in a distributed fashion, and for several premotor fields and the primary motor cortex, between-limb somatotopy (face, arm and leg) is evident. Additionally somatotopic gradients can be identified on top of an underlying distributed representation at least within the upper extremities. However, general within-limb somatotopy is clearly limited. Motor functional segregations and integrations generally parallel the biomechanical independence of and dependencies between different body parts (Schieber 2001). In sum, this well-known mixture of functional segregation and functional overlap in premotor regions builds a plausible background to our interpretation that PCG subregions contribute in a characteristically combined and weighted fashion to different functional requirements rather than being exclusively involved in only the one or the other task.

Resume

Connectivity-based cortex parcellation revealed that the human precentral gyrus (PCG) consists of four distinct subregions. This parcellation seems consistent with the assumption of four premotor fields on the lateral convexity, as assessed in the macaque monkey. Moreover, three functional MRI experiments supported the interpretation that different connectivity profiles corresponded to different functional profiles in the identified areas. Though cortex parcellation based on diffusion based tracing techniques is not free of possible artifacts and pitfalls (for discussion, cf. Anwander et al., 2007), we take our findings to encourage the application of this promising approach in other cortical regions as well.

Acknowledgments

The authors wish to thank Timm Wetzel and Enrico Kaden for acquisition and preprocessing of the diffusion-weighted MR datasets, Marcel Mücke for experimental and analytical assistance, Andrea Gast-Sandmann, Kerstin Flake and Corina Melzer for illustrations, and Uta Wolfensteller for proof reading and helpful suggestions on former versions of the manuscript.

References

Anwander, A., Tittgemeyer, M., von Cramon, D.Y., Friederici, A.D., Knosche, TR., 2007. Connectivity-based parcellation of Broca's area. Cereb. Cortex 17, 816–825.

Barbas, H., Pandya, D.N., 1987. Architecture and frontal cortical connections of the premotor cortex (area-6) in the rhesus-monkey. J. Comp. Neurol. 256, 211–228.

Behrens, T.E., Johansen-Berg, H., 2005. Relating connectional architecture to grey matter function using diffusion imaging. Philos. Trans. R. Soc. Lond. B. Biol. Sci. 360 (1457), 903–911.

Bremmer, F., Schlack, A., Shah, N.J., Zafiris, O., Kubischik, M., Hoffmann, K., Zilles, K., Fink, G.R., 2001. Polymodal motion processing in posterior parietal and premotor cortex: a human fMRI study strongly implies equivalencies between humans and monkeys. Neuron 29, 287–296.

Brodmann, K., 1909. Vergleichende Lokalisationslehre der Großhirnrinde in ihren Prinzipien dargestellt auf Grund des Zellaufbaues. Leipzig, Barth.

Buccino, G., Binkofski, F., Fink, G.R., Fadiga, L., Fogassi, L., Gallese, V., Seitz, R.J., Zilles, K., Rizzolatti, G., Freund, H.J., 2001. Action observation activates premotor and parietal areas in a somatotopic manner: an fMRI study. Eur. J. Neurosci. 13, 400–404.

Caminiti, R., Genovesio, A., Marconi, B., Mayer, A.B., Onorati, P., Ferraina, S., Mitsuda, T., Giannetti, S., Squatrito, S., Maioli, M.G., Molinari, M., 1999. Early coding of reaching: frontal and parietal association connections of parieto-occipital cortex. Eur. J. Neurosci. 11, 3339–3345.
Caspers, S., Geyer, S., Schleicher, A., Mohlberg, H., Amunts, K., Zilles, K., 2006. The human inferior parietal cortex: cytoarchitectonic parcellation and interindividual variability. Neuroimage 33, 430–448.
Colby, C., Duhamel, J., Goldberg, M., 1993. Ventral intraparietal area of the macaque: anatomic location and visual response properties. J. Neurophysiol. 69, 902–914.
Dale, A.M., Fischl, B., Sereno, M.I., 1999. Cortical surface-based analysis. I. Segmentation and surface reconstruction. Neuroimage 9, 179–194.
Duhamel, J.R., Bremmer, F., BenHamed, S., Graf, W., 1997a. Spatial invariance of visual receptive fields in parietal cortex neurons. Nature 389, 845–848.
Duhamel, J.R., Colby, C., Goldberg, M., 1997b. Ventral intraparietal area of the macaque: congruent visual and somatic properties. J. Neurophysiol. 79, 126–136.
Dum, R.P., Strick, P.L., 1991. The origin of corticospinal projections from the premotor areas in the frontal lobe. J. Neurosci. 11, 667–689.
Eickhoff, S.B., Heim, S., Zilles, K., Amunts, K., 2006. Testing anatomically specified hypotheses in functional imaging using cytoarchitectonic maps. NeuroImage 32, 570–582.
Forman, S.D., Cohen, J.D., Fitzgerald, M., Eddy, W.F., Mintun, M.A., Noll, D.C., 1995. Improved assessment of significant activation in functional magnetic resonance imaging (fMRI): use of a cluster-size threshold. Magn. Reson. Med. 33, 636–647.
Fox, P.T., Huang, A., Parsons, L.M., Xiong, J.H., Zamarippa, F., Rainey, L., Lancaster, J.L., 2001. Location-probability profiles for the mouth region of human primary motor-sensory cortex: model and validation. Neuroimage 13, 196–209.
Friederici, A.D., 2009. Pathways to language: fiber tracts in the human brain. Trends Cogn. Sci. 13, 175–181.
Friston, K.J., 1994. Statistical parametric mapping. In: Thatcher, R.W., Hallet, M., Zeffiro, T., John, E.R., Huerta, M. (Eds.), Functional neuroimaging: technical foundations. Academic Press, San Diego, pp. 79–93.
Friston, K.J., Holmes, A.P., Poline, J.B., Grasby, P.J., Williams, S.C.R., Frackowiak, R.S.J., Turner, R., 1995a. Analysis of fMRI time-series revisited. Neuroimage 2, 45–53.
Friston, K.J., Holmes, A.P., Worsley, K.J., Poline, J.P., Frith, C.D., Frackowiak, R.S.J., 1995b. Statistical parametric maps in functional imaging: a general linear approach. Hum. Brain Mapp. 2, 189–210.
FSL, "FMRIB Software Library," University of Oxford, 2006. [Online]. Available: http://www.fmrib.ox.ac.uk/fsl.
Geyer, S., 2004. The microstructural border between the motor and the cognitive domain in the human cerebral cortex. Adv. Anat. Embryol Cell. Biol. 174, 1–89.
Geyer, S., Matelli, M., Luppino, G., Zilles, K., 2000. Functional neuroanatomy of the primate isocortical motor system. Anat. Embryol (Berl) 202, 443–474.
Ghosh, S., Gattera, R., 1995. A comparison of the ipsilateral cortical projections to the dorsal and ventral subdivisions of the macaque premotor cortex. Somatosens. Mot. Res. 12, 359–378.
Godschalk, M., Lemon, R., Kuypers, H., Ronday, H., 1984. Cortical afferents and efferents of monkey postarcuate area: an anatomical and electrophysiological study. Exp. Brain Res. 56, 410–424.
Husain, M., Nachev, P., 2007. Space and the parietal cortex. Trends Cogn. Sci. 11, 30–36.
Jenkinson, M., Bannister, P., Brady, M., Smith, S., 2002. "Improved optimization for the robust and accurate linear registration and motion correction of brain images. NeuroImage 17 (2), 825–841.
Johansen-Berg, H., Behrens, T.E., Robson, M.D., Drobnjak, I., Rushworth, M.F., Brady, J.M., Smith, S.M., Higham, D.J., Matthews, P.M., 2004. Changes in connectivity profiles define functionally distinct regions in human medial frontal cortex. Proc. Natl. Acad. Sci. U. S. A. 101, 13335–13340.
Johansen-Berg, H., Behrens, T.E., 2006. Just pretty pictures? What diffusion tractography can add in clinical neuroscience. Curr. Opin. Neurol. 19, 379–385.
Keysers, C., Perrett, D.I., 2004. Demystifying social cognition: a Hebbian perspective. Trends Cogn. Sci. 8, 501–507.
Koch, M.A., Norris, D.G., Hund-Georgiadis, M., 2002. An investigation of functional and anatomical connectivity using magnetic resonance imaging. Neuroimage 16 (1), 241–250.
Lohmann, G., Müller, K., Bosch, V., Mentzel, H., Hessler, S., Chen, L., Zysset, S., Von Cramon, D.Y., 2001. Lipsia - a new software system for the evaluation of functional magnetic resonance images of the human brain. Comput. Med. Imaging Graph. 25, 449–457.
Luppino, G., Murata, A., Govoni, P., Matelli, M., 1999. Largely segregated parietofrontal connections linking rostral intraparietal cortex (areas AIP and VIP) and the ventral premotor cortex (areas F5 and F4). Exp. Brain Res. 128, 181–187.
Maioli, M.G., Squatrito, S., Samolsky-Dekel, B.G., Sanseverino, E.R., 1998. Corticocortical connections between frontal periarcuate regions and visual areas of the superior temporal sulcus and the adjoining inferior parietal lobule in the macaque monkey. Brain Res. 789, 118–125.
Marconi, B., Genovesio, A., Battaglia-Mayer, A., Ferraina, S., Squatrito, S., Molinari, M., Lacquaniti, F., Caminiti, R., 2001. Eye-hand coordination during reaching. I. Anatomical relationships between parietal and frontal cortex. Cereb. Cortex 11, 513–527.
Matelli, M., Camarda, R., Glickstein, M., Rizzolatti, G., 1986. Afferent and efferent projections of the inferior area 6 in the macaque monkey. J. Comp. Neurol. 251, 281–298.
Ono, M., Kubik, S., Abernathey, C.D., 1990. Atlas of the cerebral sulci. Stuttgart, Thieme.
Picard, N., Strick, P.L., 2001. Imaging the premotor areas. Curr. Opin. Neurobiol. 11 (6), 663–672.
Preuss, T.M., Stepniewska, I., Kaas, J.H., 1996. Movement representation in the dorsal and ventral premotor areas of owl monkeys: a microstimulation study. J. Comp. Neurol. 371, 649–676.
Rademacher, J., Caviness, V.S., Steinmetz, H., Galaburda, A.M., 1993. Topographical variation of the human primary cortices: implications for neuroimaging, brain mapping, and neurobiology. Cereb. Cortex 3, 313–329.
Rilling, J.K., Glasser, M.F., Preuss, T.M., Ma, X., Zhao, T., Hu, X., Behrens, T.E., 2008. The evolution of the arcuate fasciculus revealed with comparative DTI. Nat. Neurosci. 11 (4), 426–428.
Rizzolatti, G., 1987. Functional organization of inferior area 6. Ciba Found. Symp. 132, 171–186.
Rizzolatti, G., Craighero, L., 2004. The mirror-neuron system. Annu. Rev. Neurosci. 27, 169–192.
Rizzolatti, G., Fogassi, L., Gallese, V., 2002. Motor and cognitive functions of the ventral premotor cortex. Curr. Opin. Neurobiol. 12, 149–154.
Rizzolatti, G., Luppino, G., 2001. The cortical motor system. Neuron 31, 889–901.
Rizzolatti, G., Luppino, G., Matelli, M., 1998. The organization of the cortical motor system: new concepts. Electroencephalogr. Clin. Neurophysiol. 106, 283–296.
Roland, P.E., Zilles, K., 1996. Functions and structures of the motor cortices in humans. Curr. Opin. Neurobiol. 6, 773–781.
Rorden, C., Karnath, H.O., Bonilha, L., 2007. Improving lesion-symptom mapping. J. Cogn. Neurosci. 19 (7), 1081–1088.
Rozzi, S., Calzavara, R., Belmalih, A., Borra, E., Gregoriou, G.G., Matelli, M., Luppino, G., 2006. Cortical connections of the inferior parietal cortical convexity of the Macaque monkey. Cereb. Cortex 16, 1389–1417.
Sakreida, K., Schubotz, R.I., Wolfensteller, U., von Cramon, D.Y., 2005. Motion class dependency in observers' motor areas revealed by functional magnetic resonance imaging. J. Neurosci. 25, 1335–1342.
Schieber, M., 2001. Constraints on somatotopic organization in the primary motor cortex. J. Neurophysiol. 86 (5), 2125–2143.
Schmahmann, J.D., Pandya, D.N., Wang, R., Dai, G., D'Arceuil, H.E., de Crespigny, A.J., Wedeen, V.J., 2007. Association fibre pathways of the brain: parallel observations from diffusion spectrum imaging and autoradiography. Brain 130, 630–653.
Schubotz, R.I., 1999. Instruction differentiates the processing of temporal and spatial sequential patterns: Evidence from slow wave activity in humans. Neurosci. Lett. 265, 1–4.
Schubotz, R.I., von Cramon, D.Y., 2001. Functional organization of the lateral premotor cortex: fMRI reveals different regions activated by anticipation of object properties, location and speed. Cogn. Brain Res. 11, 97–112.
Schubotz, R.I., von Cramon, D.Y., 2002. Predicting perceptual events activates corresponding motor schemes in lateral premotor cortex: an fMRI study. Neuroimage 15 (4), 787–796.
Schubotz, R.I., von Cramon, D.Y., 2003. Functional-anatomical concepts of human premotor cortex: evidence from fMRI and PET studies. Neuroimage 20, 120–131.
Schubotz, R.I., von Cramon, D.Y., Lohmann, G., 2003. Auditory what, where, and when: a sensory somatotopy in lateral premotor cortex. NeuroImage 20, 173–185.
Schubotz, R.I., 2004. Human premotor cortex: beyond motor performance. MPI Series in Human Cognitive and Brain Sciences, Vol. 50. Max Planck Institute for Human Cognitive and Brain Sciences, Leipzig.
Schubotz, R.I., 2007. Prediction of external events with our motor system: towards a new framework. Trends Cogn. Neurosci. 11, 211–218.
Simonyan, K., Jürgens, U., 2002. Cortico-cortical projections of the motorcortical larynx area in the rhesus monkey. Brain Res. 949, 23–31.
Simonyan, K., Jürgens, U., 2005. Afferent cortical connections of the motor cortical larynx area in the rhesus monkey. Neuroscience 130, 133–149.
Talairach, J., Tournoux, P., 1988. Co-planar stereotaxis atlas of the human brain. Thieme, New York.
Tanne-Gariepy, J., Rouiller, E., Boussaoud, D., 2002. Parietal inputs to dorsal versus ventral premotor areas in the macaque monkey: evidence for largely segregated visuomotor pathways. Exp. Brain Res. 145, 91–103.
Tomassini, V., Jbabdi, S., Klein, J.C., Behrens, T.E., Pozzilli, C., Matthews, P.M., Rushworth, MF., Johansen-Berg, H., 2007. Diffusion-weighted imaging tractography-based parcellation of the human lateral premotor cortex identifies dorsal and ventral subregions with anatomical and functional specializations. J. Neurosci. 27 (38), 10259–10269.
Vogt C, Vogt O. 1919. Zur Kenntnis der pathologischen Veränderungen des Striatum und des Pallidum und zur Pathophysiologie der dabei auftretenden Krankheit-serscheinungen. Heidelberg. Sitzungsberichte der Heidelberger Akademie der Wissenschaften. Mathematisch-naturwissenschaftliche Klasse.
Wolfensteller, U., Schubotz, R.I., von Cramon, D.Y., 2007. Understanding non-biological dynamics with your own premotor system. Neuroimage 36 (Suppl. 2), T33–43.
Worsley, K.J., Friston, K.J., 1995. Analysis of fMRI time-series revisited—again. Neuroimage 2, 173–181.
Yousry, T.A., Schmid, U.D., Alkadhi, H., Schmidt, D., Peraud, A., Buettner, A., Winkler, P., 1997. Localization of the motor hand area to a knob on the precentral gyrus. A new landmark. Brain 120, 141–157.